Amorphous-to-$Cu_{51}Zr_{14}$ phase transformation in $Cu_{60}Ti_{20}Zr_{20}$ alloy

2003 J. Phys.: Condens. Matter 15 8703

(http://iopscience.iop.org/0953-8984/15/50/004)

INSTITUTE OF PHYSICS PUBLISHING JOURNAL OF PHYSICS: CONDENSED MATTER

J. Phys.: Condens. Matter **15** (2003) 8703–8712 PII: S0953-8984(03)67110-9

Amorphous-to-$Cu_{51}Zr_{14}$ phase transformation in $Cu_{60}Ti_{20}Zr_{20}$ alloy

Q P Cao[1,2], Y H Zhou[2], A Horsewell[3] and J Z Jiang[1,4,5]

[1] Department of Physics, Building 307, Technical University of Denmark, DK-2800 Lyngby, Denmark
[2] School of Materials Science and Engineering, Shanghai Jiao Tong University, Shanghai, 200030, People's Republic of China
[3] Department of Manufacturing Engineering and Management, Building 204, Technical University of Denmark, DK-2800 Lyngby, Denmark
[4] Department of Materials Science and Engineering, Zhejiang University, Hangzhou 310027, People's Republic of China

E-mail: jiang@fysik.dtu.dk

Received 4 August 2003
Published 3 December 2003
Online at stacks.iop.org/JPhysCM/15/8703

Abstract

The kinetics of an amorphous-to-$Cu_{51}Zr_{14}$ phase transformation in an as-cast $Cu_{60}Ti_{20}Zr_{20}$ rod have been investigated by differential scanning calorimetry. The relative volume fractions of the transferred crystalline phase as a function of annealing time, obtained at 713, 716, 723, 728, and 733 K, have been analysed in detail using 14 nucleation and growth models together with the JMA model. A time-dependent nucleation process is revealed. A steady-state nucleation rate of the order of 10^{22}–10^{23} nuclei m^{-3} s^{-1} in the temperature range 713–733 K and an activation energy of the order of 550 kJ mol^{-1} for the phase transformation in the as-cast $Cu_{60}Ti_{20}Zr_{20}$ rod were detected, for which some possible reasons are suggested.

1. Introduction

The first Cu-rich bulk metallic glass-forming alloys were discovered in a Cu–Ti–Zr–Ni system [1], and then Cu–Ti–Zr–Ni–Si and Cu–Ti–Zr–Ni–Sn systems were reported [2, 3]. Very recently, the report of ternary $Cu_{60}Ti_{10}Zr_{30}$ and $Cu_{60}Ti_{15}Hf_{25}$ systems [4, 5], exhibiting excellent mechanical properties, has generated considerable research activity in this area [4–28], especially in the microstructure of the ternary systems which is essential to explain the excellent mechanical properties [4–14]. For the $Cu_{60}Ti_{10+x}Zr_{30-x}$ ($x = 0$ and 10) alloys, the existence of nanocrystals was confirmed in as-prepared ribbon and rod samples by electron microscopy [8–10]. The differential scanning calorimeter (DSC) measurements reveal two

[5] Author to whom any correspondence should be addressed.

exothermic peaks assigned to an amorphous-to-$Cu_{51}Zr_{14}$ phase transition and the formation of a $MgZn_2$-type hexagonal phase [11–13]. The origin of non-detectable x-ray diffraction (XRD) peaks in the annealed samples with a large reduction of the first exothermic peak area was uncovered due to overlapping of diffraction peaks of $Cu_{51}Zr_{14}$ phase with small crystallite sizes and defects [12]. Here we report the kinetics of the amorphous-to-$Cu_{51}Zr_{14}$ phase transformation in as-cast $Cu_{60}Ti_{20}Zr_{20}$ rod.

2. Experimental details

Alloy ingots with the composition of $Cu_{60}Ti_{20}Zr_{20}$ were prepared by arc melting pure metals of 99.99% copper, 99.9% zirconium and 99.9% titanium in a purified argon atmosphere. Cylindrical $Cu_{60}Ti_{20}Zr_{20}$ samples of 2 mm diameter were prepared by a copper mould casting method. The XRD measurements were performed using a Philips PW 1820 diffractometer with Cu Kα radiation. Thermal analyses were performed in a Pyris Diamond power compensation DSC at a heating rate of 20 K min^{-1} under a flow of purified argon (99.998%). The samples were placed in Al pans. The DSC equipment was calibrated to within 0.5 K using melting of relevant pure metals. Isothermal measurements were performed by heating samples to a given temperature at a rate of 20 K min^{-1}. It should be noted that at 20 K min^{-1} the difference between sample and DSC programmed temperatures at any time is negligible, while high heating rates could cause a big difference, e.g., around 5 K difference for 100 K min^{-1}. Heat treatments were carried out in the DSC machine by first heating the sample to a given temperature at 20 K min^{-1}, maintaining the temperature for various times and finally cooling down using a rate of 200 K min^{-1}. The DSC measurements of the annealed samples were carried out just after the heat treatments.

3. Results and discussion

Figures 1 and 2 show DSC curves and the time dependence of the first and second exothermic peak areas for the as-cast and annealed $Cu_{60}Ti_{20}Zr_{20}$ rods at 708 K. The DSC curve for the as-cast rod exhibits an endothermic event, characterized by a glass transition temperature $T_g = 706$ K, followed by two exothermic events, indicating a two-stage phase transformation process, characterized by $T_{x1} = 736$ K, $\Delta H_1 = 19 \pm 1$ J g^{-1} and $T_{x2} = 767$ K, $\Delta H_2 = 28 \pm 1$ J g^{-1}, which are in good agreement with data reported in the literature [11–13]. Upon increasing the annealing time, the enthalpy of the first exothermic peak monotonically decreases from 19 J g^{-1} for the as-cast rod to close to 0 J g^{-1} for the sample annealed for 2.4 ks, while the second exothermic peak remains almost unchanged within experimental uncertainty up to 5.4 ks. With further increases in the annealing time, the second exothermic peak starts to decrease and becomes very small after 43.2 ks. We further performed XRD measurements of the corresponding samples after the isothermal annealing treatments at 708 K, as shown in figure 3. Similar to the as-cast $Cu_{60}Ti_{10}Zr_{30}$ rod [12], no diffraction Bragg peaks from the $Cu_{51}Zr_{14}$ phase were detected after 2.4 ks, at which the first exothermic peak almost disappears. However, the FWHM of the peak located at $2\theta \approx 41°$ in figure 4, deduced from both Gauss and Lorentz line profiles, does decrease by about 25% from the as-cast rod to the sample annealed for 2.4 ks. After 5.4 ks peaks from the $Cu_{51}Zr_{14}$ phase appear, and after 43.2 ks the diffraction pattern is dominated by the diffraction peaks of $Cu_{51}Zr_{14}$ phase. The drop in integrated intensity by about 94% of the second exothermic peak area after 43.2 ks as compared to as-cast rod indicates that the grain growth of the second $MgZn_2$-type phase is much slower at 708 K so that the crystallite size of the second crystalline phase could be too small to be detected by

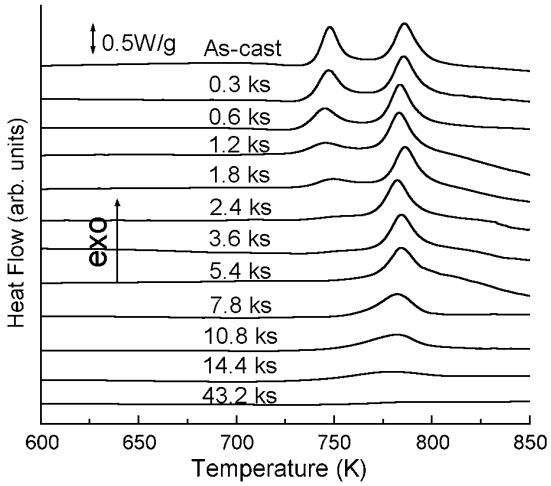

Figure 1. DSC curves for the as-cast $Cu_{60}Ti_{20}Zr_{20}$ rod and samples annealed at 708 K for various times in DSC, at a heating rate of 20 K min^{-1} under a flow of purified argon.

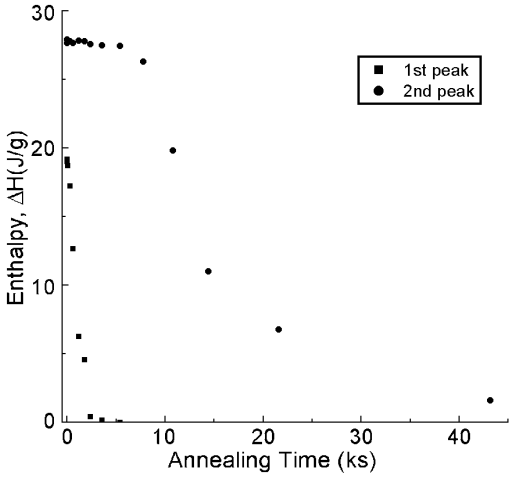

Figure 2. The time dependence of the first and second exothermic peak areas for the as-cast $Cu_{60}Ti_{20}Zr_{20}$ rod and samples annealed at 708 K for various times in DSC.

XRD. In order to check the nature of the second exothermic peak, we heated the sample at 20 K min^{-1} to 813 and 853 K and cooled at a rate of 200 K min^{-1}. The XRD patterns recorded for the two samples are shown in figure 5. It is clear that after 853 K, which is higher than the second exothermic peak, the $MgZn_2$-type phase appears together with the $Cu_{51}Zr_{14}$ phase. Based on the results mentioned above and the results reported in [10–13], we could conclude that for the first crystallization event, the amorphous-to-$Cu_{51}Zr_{14}$ phase transition, the XRD technique is not able to detect the transformation, while DSC is much more sensitive to it.

Figure 6 depicts isothermal DSC thermograms of the first crystallization event at 713, 718, 723, 728, and 733 K for the as-cast $Cu_{60}Ti_{20}Zr_{20}$ rod. To be sure that the heat release observed in figure 6 is only from the first crystallization reaction, we further performed constant heating DSC measurements for the samples after the isothermal measurements and found that the areas of the second exothermic peak were equal to that for the as-cast rod without isothermal measurements. When we assume that the heat release measured in figure 6 is proportional to the volume of the transferred phase, then the relative volume fraction of the $Cu_{51}Zr_{14}$ phase as a function of time can be deduced, as shown in figure 7. The shape of the curves is a typical 'S' type.

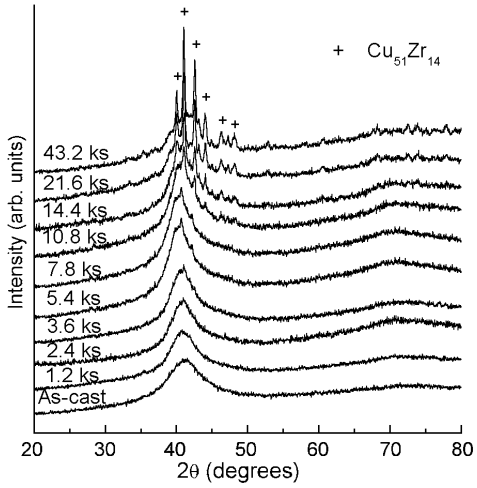

Figure 3. X-ray diffraction patterns recorded for the as-cast $Cu_{60}Ti_{20}Zr_{20}$ rod and samples annealed at 708 K for various times in DSC.

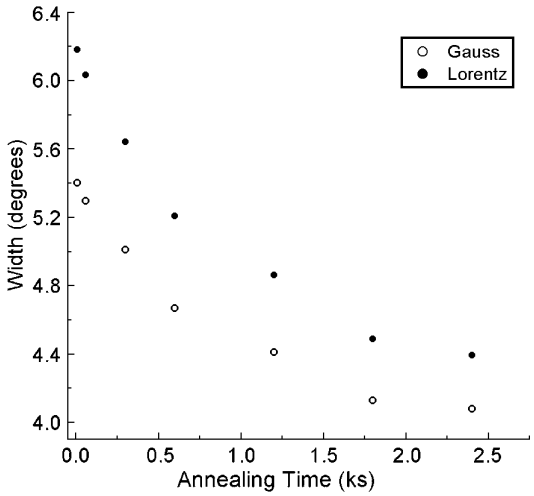

Figure 4. The FWHM of the peak located at $2\theta \approx 41°$ using both Lorentz and Gauss line profiles, as a function of annealing time for as-cast $Cu_{60}Ti_{20}Zr_{20}$ rod and samples annealed at 708 K for various times in DSC.

In many cases, the time evolution of the fraction of a phase is represented by a phenomenological model describing the kinetics of isothermal phase transformation, known as the Johnson–Mehl–Avrami (JMA) model [29–31]. The essence of the model can be written as a very simple formula commonly referred to as the JMA equation

$$x(t) = 1 - \exp\{-[k(t-\tau)]^n\} \tag{1}$$

where $x(t)$ is the volume fraction of the transformed phase, t the annealing time, n a constant related to the dimensionality of nucleation and growth, k a kinetic constant of the process which depends on temperature and effective activation energy, E_a, by $k = k_0 \exp(-E_a/RT)$, where k_0 is a constant and R is the gas constant, and τ the incubation time, which can be expressed as $\tau = \tau_0 \exp(E_a/RT)$, where τ_0 is a constant. Equation (1) can fit the experimental results well, as shown in figure 7 by solid curves, for annealing times longer than τ. The values of k, τ and n obtained from the fitting are listed in table 1. Both k and n are good experimental parameters for kinetic studies and are usually estimated from the intercept and slope, respectively, of a $\ln[-\ln(1-x)]$ versus $\ln(t-\tau)$ plot for a limited experimental data, providing the value of τ. Figure 8 shows the plot of $\ln[-\ln(1-x)]$ versus $\ln(t-\tau)$ at five temperatures for the

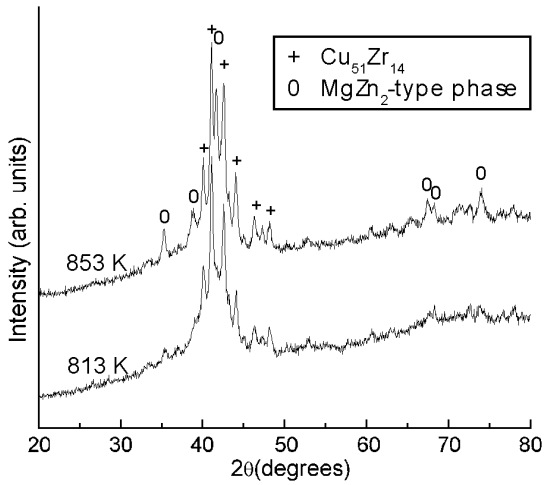

Figure 5. X-ray diffraction patterns recorded for as-cast $Cu_{60}Ti_{20}Zr_{20}$ samples heated up to 813 and 853 K in DSC using a rate of 20 K min^{-1} under a flow of purified argon.

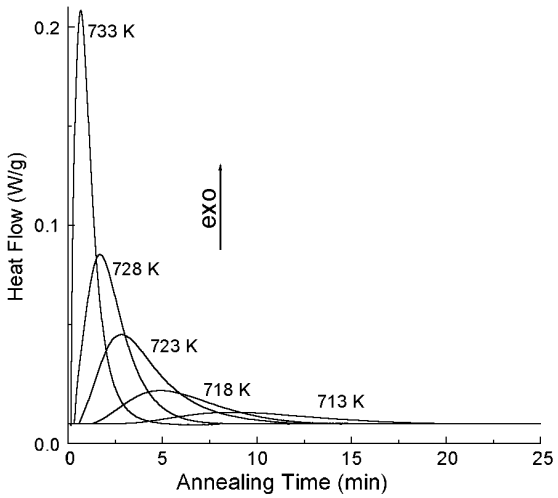

Figure 6. Isothermal DSC thermograms of the first crystallization event at 713, 718, 723, 728, and 733 K for as-cast $Cu_{60}Ti_{20}Zr_{20}$ rod.

data of $x = 0.2$–0.8, in which the values of τ obtained from equation (1) are used. The values of k and n deduced from the slopes and intercepts are also listed in table 1, which are in accordance with those obtained directly from equation (1). The effective activation energy for the formation of $Cu_{51}Zr_{14}$ phase from the as-cast $Cu_{60}Ti_{20}Zr_{20}$ rod is found to be 490 ± 50 or 533 ± 24 kJ mol^{-1}, deduced from the plots of $\ln k$ versus $1/T$ or $\ln \tau$ versus $1/T$ as shown in figure 9, respectively. Both methods give almost the same values for the effective activation energy within experimental uncertainty, which are very large. A similar value was also deduced from Kissinger plots for an as-spun $Cu_{60}Ti_{20}Zr_{20}$ ribbon [13]. The higher the effective activation energy the higher the effective energy barrier for the nucleation and growth process.

It is clear from figure 7 that

(1) volume fractions of the $Cu_{51}Zr_{14}$ phase detectable by DSC require incubation times at all five temperatures used here and
(2) the JMA model cannot describe the data for annealing times less than the incubation times.

These results imply the existence of a transient nucleation process for the amorphous-to-$Cu_{51}Zr_{14}$ phase transformation in the as-cast $Cu_{60}Ti_{20}Zr_{20}$ rod. Furthermore, it was reported

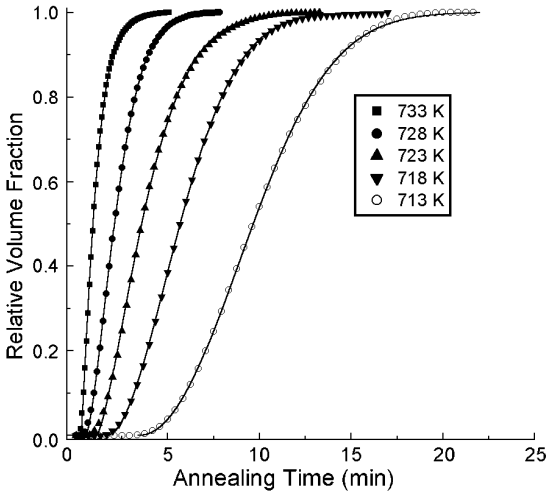

Figure 7. Relative volume fractions of the $Cu_{51}Zr_{14}$ phase as a function of time at 713, 718, 723, 728, and 733 K for the as-cast $Cu_{60}Ti_{20}Zr_{20}$ rod. Points are the data deduced from figure 6 and solid curves are the fits from the JMA equation.

Table 1. Parameters obtained from the JMA model, model 8 and model 10 at five temperatures for the as-cast $Cu_{60}Ti_{20}Zr_{20}$ rod.

	Parameters	713 K	718 K	723 K	728 K	733 K
	k (min^{-1})	0.134 ± 0.001	0.207 ± 0.001	0.316 ± 0.002	0.502 ± 0.002	1.134 ± 0.005
From	τ (min)	3.36 ± 0.01	1.71 ± 0.01	1.12 ± 0.02	0.53 ± 0.01	0.28 ± 0.01
figure 7	n	2.1 ± 0.1	1.8 ± 0.1	1.5 ± 0.2	1.6 ± 0.2	1.2 ± 0.3
	E_a (kJ mol^{-1})			533 ± 24		
From	k (min^{-1})	0.136 ± 0.002	0.208 ± 0.002	0.317 ± 0.002	0.503 ± 0.002	1.136 ± 0.002
figure 8	n	2.1 ± 0.1	1.9 ± 0.1	1.5 ± 0.2	1.6 ± 0.1	1.3 ± 0.2
From	$I_{st\text{-}K} V_0$ (min^{-1})	0.61 ± 0.03	0.60 ± 0.02	0.57 ± 0.01	0.94 ± 0.03	1.51 ± 0.02
model	τ_K (min)	8.5 ± 0.5	3.7 ± 0.3	1.7 ± 0.4	0.9 ± 0.2	0.3 ± 0.1
8	E_K (kJ mol^{-1})			582 ± 83		
From	$I_{st\text{-}Z} V_0$ (min^{-1})	1.39 ± 0.01	1.14 ± 0.02	0.91 ± 0.02	1.47 ± 0.05	2.08 ± 0.02
model	τ_Z (min)	17.0 ± 0.8	6.9 ± 0.9	2.8 ± 0.7	1.5 ± 0.6	0.4 ± 0.2
10	E_Z (kJ mol^{-1})			600 ± 125		

that the grain size of the $Cu_{51}Zr_{14}$ phase, formed during isothermal annealing treatments in the supercooled liquid region for the $Cu_{60}Ti_{20-x}Zr_{20+x}$ ($x = 0$ and 10) alloys, is very small, approximately 5–10 nm [10, 12, 13]. Thus, to confirm the high value of the activation energy for the amorphous-to-$Cu_{51}Zr_{14}$ phase transformation, we attempt to analyse the kinetic data obtained here using various nucleation and growth models. Time-dependent nucleation, or transient nucleation, means that over time an equilibrium cluster distribution is established [32]. Due to fast nucleation processes in metallic glasses, in general, steady-state nucleation has been considered in most cases. In the classic transient nucleation theory, two analyses, based on the Zeldovich–Frenkel equation [33], were proposed. One is the Zeldovich equation (hereafter Z-model). Zeldovich [33] assumed that the work of formation of a nucleus with size d is proportional to d^2 and the rate of monomer addition to a nucleus with size d is $k_d^+ \approx k_{d^*}^+$, and found a time-dependent nucleation rate, $I_{d^*}(t)$, at the critical size d^* as

$$I_{d^*} = I_{st\text{-}Z} \exp(-\tau_Z/t) \tag{2}$$

where τ_Z is the transient nucleation time and $I_{st\text{-}Z}$ is the steady-state nucleation rate for the Z-model. The other is the Kashchiev equation (hereafter K-model) [34]. Kashchiev further

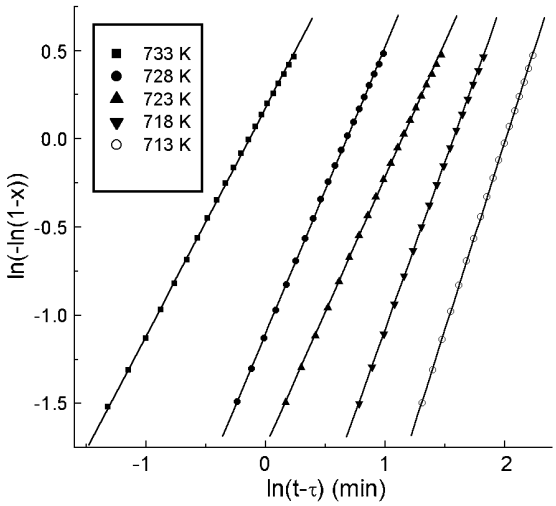

Figure 8. JMA plots, $\ln[-\ln(1-x)]$ versus $\ln(t-\tau)$, at five temperatures for the as-cast $Cu_{60}Ti_{20}Zr_{20}$ rod, in which the data for $0.2 < x < 0.8$ are used.

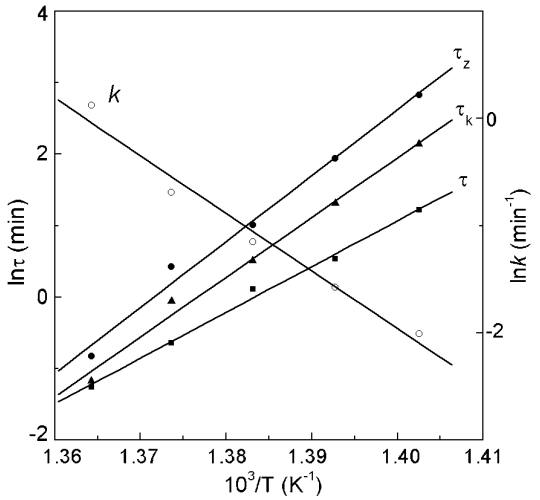

Figure 9. Arrhenius plots of induction time, τ, and effective rate constant, k, as a function of temperature for the amorphous-to-$Cu_{51}Zr_{14}$ phase transformation in the as-cast $Cu_{60}Ti_{20}Zr_{20}$ rod, in which k values obtained from JMA and τ values obtained from JMA and models 8 and 10, listed in table 1, are used.

studied the transient nucleation process and performed the most thorough analytical treatment of the Zeldovich–Frenkel equation. Based on two assumptions, (1) the work of formation of a nucleus with size d is approximated by the first two non-zero terms in a Taylor expansion about d^*, and (2) $k_d^+ \approx k_{d^*}^+$, he derived the time-dependent nucleation rate as

$$I_{d^*} = I_{\text{st-K}}\left[1 + 2\sum_{m=1}^{\infty}(-1)^m \exp\left(-\frac{m^2 t}{\tau_{\text{K}}}\right)\right] \tag{3}$$

where τ_{K} is the transient nucleation time and $I_{\text{st-K}}$ is the steady-state nucleation rate for the K-model. The relative crystallized volume fraction $x(t)$ during the crystallization process in metallic glasses as a function of time can be expressed as $x(t) = 1 - \exp(-Y(t))$, where the expression of $Y(t)$ depends on the nucleation and growth models used. In our previous work [35], 14 different nucleation and growth models have been established. They are

(1) quenched-in nucleation with three-dimensional constant growth rate U;
(2) quenched-in nucleation with constant grain size V_0;

(3) steady-state nucleation I_{st} with three-dimensional constant growth rate;
(4) steady-state nucleation with constant grain size;
(5) quenched-in and steady-state nucleation with constant growth rate;
(6) quenched-in and steady-state nucleation with constant grain size;
(7) time-dependent K-model with three-dimensional constant growth rate;
(8) time-dependent K-model with constant grain size;
(9) time-dependent Z-model with three-dimensional constant growth rate;
(10) time-dependent Z-model with constant grain size;
(11) time-dependent K-model with three-dimensional constant growth rate at $t < t_0$ and zero growth rate at $t > t_0$;
(12) time-dependent Z-model with three-dimensional constant growth rate at $t < t_0$ and zero growth rate at $t > t_0$;
(13) quenched-in and time-dependent Z-model with three-dimensional constant growth rate; and
(14) quenched-in and time-dependent Z-model with constant grain size.

We found that the relative volume fraction data versus time can be well fitted using either the Z- or K-model with a constant grain size while the steady-state nucleation process cannot describe the experimental data for the amorphous-to-$Cu_{51}Zr_{14}$ phase transformation in the as-cast $Cu_{60}Ti_{20}Zr_{20}$ rod, as shown in figure 10. The initial transition stage can be well fitted using the models, as illustrated in the inset. The deduced parameters using models 8 and 10 are listed in table 1. Three striking features are found.

(1) The activation energies, deduced from the incubation time for both K- and Z-models, of the amorphous-to-$Cu_{51}Zr_{14}$ phase transformation in the as-cast $Cu_{60}Ti_{20}Zr_{20}$ rod are consistent with the value deduced from the JMA fitting within the uncertainty. They are indeed large values.
(2) τ_Z is about twice τ_K. The incubation time decreases as temperature increases. The incubation times are very significant in the whole phase transition time period, i.e., time-dependent nucleation must be considered for the amorphous-to-$Cu_{51}Zr_{14}$ phase transformation in the as-cast $Cu_{60}Ti_{20}Zr_{20}$ rod. A similar conclusion was also drawn for crystallization in other metallic glass systems [35–37].
(3) If we assume an average grain size of 7 nm of the $Cu_{51}Zr_{14}$ phase and use the results deduced from model 8, the steady-state nucleation rates are estimated to be $5.7 \pm 0.9 \times 10^{22}$, $5.6 \pm 0.9 \times 10^{22}$, $5.3 \pm 0.9 \times 10^{22}$, $8.7 \pm 0.9 \times 10^{22}$, and $1.4 \pm 0.9 \times 10^{23}$ nuclei m^{-3} s^{-1} at 713, 718, 723, 728, and 733 K, respectively. These values are very large, which results in the nanostructure feature in the partially crystallized $Cu_{60}Ti_{20}Zr_{20}$ rod.

Two questions we will further discuss are (1) why the system has a high steady-state nucleation rate and (2) why the activation energy for the amorphous-to-$Cu_{51}Zr_{14}$ phase transformation is extremely large. For the first question, two possible reasons came to us. In the as-cast $Cu_{60}Ti_{20}Zr_{20}$ rod, about 1000 ppm oxygen, most likely introduced by Ti and Zr elements, was found. Oxygen could act as a heterogeneous nucleation site to enhance the steady-state nucleation rate. We roughly estimated the heterogeneous nucleation site density using an embryo size of 0.5 nm ZrO_2 (or TiO_2) for 1000 ppm oxygen. The density is about 10^{26} embryo m^{-3}, which could be a source for the high steady-state nucleation rate. The second reason could be phase decomposition (separation) before crystallization in the $Cu_{60}Ti_{20}Zr_{20}$ system, which was suggested in [13] although the issue still remains to be debated fully. At boundaries between the separated phases the nucleation rate could be very high. This could result in a high steady-state nucleation rate in the system. For the second

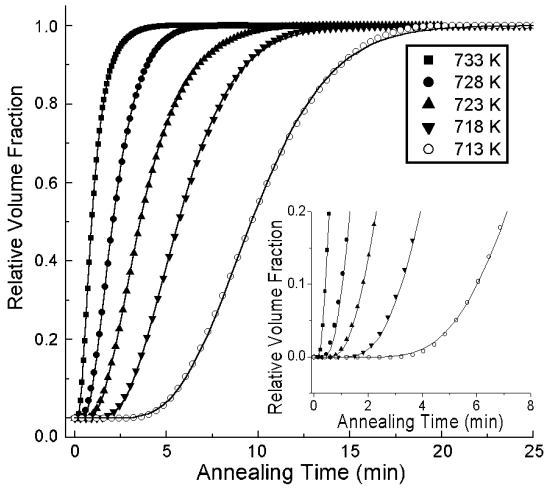

Figure 10. Relative volume fractions of the $Cu_{51}Zr_{14}$ phase as a function of time at five temperatures for the as-cast $Cu_{60}Ti_{20}Zr_{20}$ rod. The solid lines are the fitting curves using model 8 (details given in text) and points are the data deduced from figure 6. The inset illustrates the initial stage of the phase transformation.

question, the experimental fact that very small grains are observed after the first crystallization reaction indicates that the growth process is extremely slow. The first crystallites are mainly composed of Cu and Zr, implying that Ti atoms should diffuse out the region where the $Cu_{51}Zr_{14}$ phase was formed. An activation energy for Ti atom diffusion at around the glass transition temperature in a $Zr_{41.2}Ti_{13.8}Cu_{12.5}Ni_{10}Be_{22.5}$ alloy was reported to be 4.09 ± 0.76 eV, i.e., about 409 kJ mol^{-1} [38]. Amorphous boundary regions, which have a different composition to the newly formed crystalline grains, separate the grains and could act as a barrier against atomic transport. As suggested by Tang *et al* [39] and recently reviewed [40], diffusion in amorphous metallic alloys requires thermally activated highly collective atomic processes involving groups of atoms. Consequently, one expects a high activation energy for the growth process, as observed for the amorphous-to-$Cu_{51}Zr_{14}$ phase transformation in the as-cast $Cu_{60}Ti_{20}Zr_{20}$ rod.

Acknowledgments

Financial support from the Danish Technical Research Council, the Danish Natural Sciences Research Council, the National Natural Science Foundation of China (Grant 500 71032) and the DANIDA Fellowship Centre is gratefully acknowledged. We wish to thank F Faupel and K Ratzke for the discussion on diffusion.

References

[1] Lin X H and Johnson W L 1995 *J. Appl. Phys.* **78** 6514
[2] Zhang T and Inoue A 1999 *Mater. Trans. JIM* **40** 301
[3] Li C, Saida J, Kiminami M and Inoue A 2000 *J. Non-Cryst. Solids* **261** 108
[4] Inoue A, Zhang W, Zhang T and Kurosaka K 2001 *Mater. Trans. JIM* **42** 1149
[5] Inoue A, Zhang W, Zhang T and Kurosaka K 2001 *Acta Mater.* **49** 2645
[6] Louzguine D V and Inoue A 2002 *J. Mater. Res.* **17** 2112
[7] Louzguine D V and Inoue A 2002 *Appl. Phys. Lett.* **81** 2561
[8] Kasai M, Saida J, Matsushita M, Ohsuna T, Matsubara E and Inoue A 2002 *J. Phys.: Condens. Matter* **14** 13867
[9] Chen Y T, Zhang T, Zhang W, Ping D H, Hono K, Inoue A and Sakurai T 2002 *Mater. Trans. JIM* **43** 2647
[10] Jiang J Z, Saida J, Kato H, Ohsuna T and Inoue A 2003 *Appl. Phys. Lett.* **82** 4041
[11] Jiang J Z, Yang B, Saksl K, Franz H and Pryds N 2003 *J. Mater. Res.* **18** 895
[12] Jiang J Z, Kato H, Ohsuna T, Saida J, Inoue A, Saksl K, Franz H and Ståhl K 2003 *Appl. Phys. Lett.* **83** 3299
[13] Concustell A, Revesz A, Surinach S, Baro M D, Varga L K and Heunen G 2003 *J. Mater. Res.* at press

[14] For example see *RQ11 Proc. (Oxford, Aug. 2002)* 2002
[15] Inoue A, Zhang W, Zhang T and Kurosaka K 2002 *J. Non-Cryst. Solids* **304** 200
[16] Zhang W, Ishihara S and Inoue A 2002 *Mater. Trans. JIM* **43** 1767
[17] Zhang T, Yamamoto T and Inoue A 2002 *Mater. Trans. JIM* **43** 3222
[18] Zhang T and Inoue A 2002 *Mater. Trans. JIM* **43** 1367
[19] Sordelet D J, Rozhkova E, Huang P, Wheelock P B, Besser M F, Kramer M J, Clavo-Dahlborg M and Dahlborg U 2002 *J. Mater. Res.* **17** 186
[20] Park E S, Lim H K, Kim W T and Kim D H 2002 *J. Non-Cryst. Solids* **298** 15
[21] Bae D H, Lim H K, Kim S H, Kim D H and Kim W T 2002 *Acta Mater.* **50** 1749
[22] Calin M, Eckert J and Schultz L 2003 *Scr. Mater.* **48** 653
[23] Sordelet D J, Rozhkova E, Besser M F and Kramer M J 2003 *J. Non-Cryst. Solids* **317** 137
[24] Shindo T, Waseda Y and Inoue A 2003 *Mater. Trans. JIM* **44** 351
[25] Louzguine D V and Inoue A 2003 *Phil. Mag. Lett.* **83** 191
[26] Louzguine D V and Inoue A 2003 *Scr. Mater.* **48** 1325
[27] Zhang Q S, Zhang H F, Deng Y F, Ding B Z and Hu Z Q 2003 *Scr. Mater.* **49** 273
[28] Inoue A and Zhang W 2003 *J. Mater. Res.* **18** 1435
[29] Johnson W A and Mehl R F 1939 *Trans. Am. Inst. Min. Metall. Pet. Eng.* **135** 416
[30] Avrami M 1941 *J. Chem. Phys.* **9** 177
[31] Yinnon H and Uhlmann D R 1983 *J. Non-Cryst. Solids* **54** 253
[32] For example see Kelton K F 1991 *Solid State Phys.* **45** 75
[33] Zeldovich J B 1943 *Acta Physicochim. URSS* **18** 1
Frenckel J I 1946 *Kinetic Theory of Liquids* (London: Oxford University Press)
[34] Kashchiev D 1969 *Surf. Sci.* **14** 209
[35] Jiang J Z, Zhuang Y X, Rasmussen H, Saida J and Inoue A 2001 *Phys. Rev.* B **64** 094208
[36] Zhuang Y X, Jiang J Z, Lin Z G, Mezouar M, Crichton W and Inoue A 2001 *Appl. Phys. Lett.* **79** 743
[37] Jiang J Z, Jensen C H and Rasmussen A R 2003 *J. Metastable Nanocryst. Mater.* **15/16** 81
[38] Loffler J F and Johnson W L 2000 *Appl. Phys. Lett.* **76** 3395
[39] Tang X P, Geyer U, Busch R, Johnson W L and Wu Y 1999 *Nature* **402** 160
[40] Faupel F, Frank W, Macht M P, Mehrer H, Naundorf V, Ratzke K, Schober H R, Sharma S K and Teichler H 2003 *Rev. Mod. Phys.* **75** 237